ELSEVIER

Journal of Power Sources 60 (1996) 239–247

JOURNAL OF POWER SOURCES

Electric double-layer capacitor using organic electrolyte

T. Morimoto [a], K. Hiratsuka [a], Y. Sanada [a], K. Kurihara [b]

[a] *Asahi Glass Co. Ltd., Research Center, Hazawa-cho, Kanagawa-ku, Yokohama 221, Japan*

[b] *Elna Co., Ltd., Tsujido-shinmachi, Fujisawa-city, Kanagawa 251, Japan*

Received 27 January 1995

Abstract

Electric double-layer capacitors (EDLCs) based on charge storage at the interface between a high surface area carbon electrode and a propylene carbonate solution are widely used as maintenance-free power sources for IC memories and microcomputers. New applications for electric double-layer capacitors have been recently proposed. The popularity of these devices is derived from their high energy density relative to conventional capacitors and their long cycle life and high power density relative to batteries. The performance of the capacitor depends not only on the material used but also on the construction of the cells. The material, construction and performance of coin-type capacitors for memory protection and power capacitors for large power sources are described.

Keywords: Electric double-layer capacitors; Organic electrolytes; Quaternary phosphonium; Activated carbon

1. Introduction

A new electric double-layer capacitor (EDLC) based on the charge stored at the interface between a high surface area carbon electrode and an organic electrolyte solution has been developed [1], and is widely used as a maintenance-free power source for IC memories and microcomputers. The achievement of the excellent performance of the capacitor requires: (i) an electrode fabricated with high surface area activated carbon of suitable surface properties and pore geometry; (ii) an electrolyte solution which provides high conductivities over a wide temperature range and good electrochemical stabilities to allow the capacitor to be operated at high voltages, and (iii) a cell construction material which does not corrode electrochemically during anodic polarization.

New applications for electric double-layer capacitors have been proposed in recent years. The popularity of these devices is derived from their high energy density compared with conventional capacitors and their long cycle life and high power density compared with batteries. Electric double-layer capacitors exhibit virtually unlimited cycle life and maintenance-free operation as an alternative to batteries in power circuits.

The performance of the capacitors depends not only on the materials used but also on the construction of the cell. This paper reviews data of the materials, the construction and the performance of coin-type capacitors already published. The construction and the performance of power capacitors for power sources are also discussed.

2. Coin-type capacitor

2.1. Construction

Fig. 1 shows a representative structure of the electric double-layer capacitor. A unit cell of the capacitor consists of a

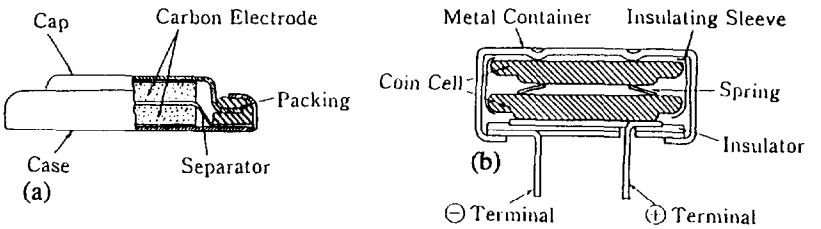

Fig. 1. Structures of EDLC using organic electrolyte solution: (a) coin cell, and (b) two-cell stacked device.

SSDI 0378-7753(95)02289-1

pair of electrodes, an organic electrolyte, a micro-porous separator and a gasket ring. These are housed in a coin-shaped electrochemically corrosion-resistant alloy container. The breakdown voltage of the unit cell is about 3.0 V, which is determined by the decomposition voltage of the electrolyte or dissolution potential of the alloy container. Therefore, two unit cells are stacked in series to get the rated voltage of 5.5 V. The stacked cells are packaged in a metal container as shown in Fig. 1.

2.2. Materials

2.2.1. Electrolyte

As the breakdown voltage of the capacitor is strongly related to the decomposition voltage of the electrolyte, it is important to use organic electrolytes with a high decomposition voltage to obtain a capacitor of both stable performance and high energy density [2,3].

Electrolyte solutions were prepared by dissolving quaternary phosphonium (R_4P^+), quaternary ammonium (R_4N^+) and lithium salts of the highest grade available in propylene carbonate (PC) distilled under low pressure and removing water by bubbling dry N_2. Anode and cathode capacitances and their combined cell capacitance were measured using a sandwich-type model cell in a glass vessel filled with the electrolyte as shown in Fig. 2. Both the anode and the cathode were carbon sheets (diameter: 12 mm, thickness: 0.5 mm) composed of activated carbon, carbon black and polytetrafluoroethylene (PTFE). The potentials of the anode and the cathode were referred to a larger carbon sheet electrode composed of the same materials as those of the two electrodes. The cell capacitance was estimated from the voltage decay during discharge from 2 to 0 V assuming that the voltage reduces linearly with time. The anode and cathode capacitances were estimated similarly from the anode and cathode potential profiles, respectively. To evaluate the electrochemical stability of the electrolyte, a practical coin cell capacitor (diameter: 18.4 mm, thickness; 2.0 mm) composed of the same electrode materials and the electrolyte, as described before, was fabricated.

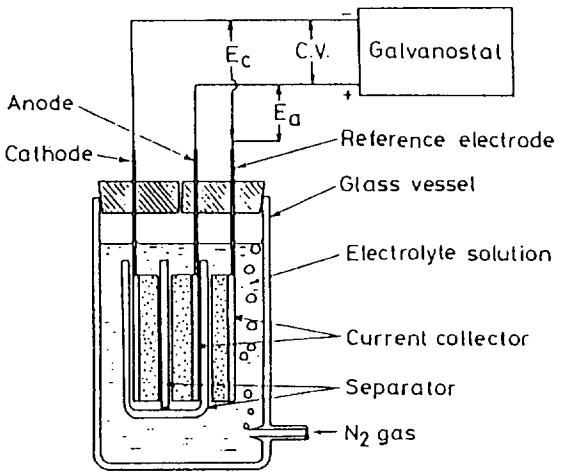

Fig. 2. Model cell for capacitance measurement.

Fig. 3 shows the cell voltage and potential curves of anode and cathode during charging and discharging at constant current of 2 mA obtained with the sandwich-type model cell in various R_4PBF_4/PC solutions. The dependencies of the capacitances in R_4P^+ and R_4N^+ salts solutions on the systematic change of substituent R were investigated. Table 1 summarizes the results of estimated capacitances obtained in the model cell. It was found that the cathode capacitance in R_4PBF_4/PC or R_4NBF_4/PC decreased with increases in the size of substituent R, whereas the anode capacitance remained almost constant. On the other hand, the cathode capacitances in the solutions containing the same cation were observed to be almost the same. $(C_2H_5)_4PBF_4$, $(C_2H_5)_4NBF_4$ and lithium salt solutions exhibited larger capacitances compared with the others.

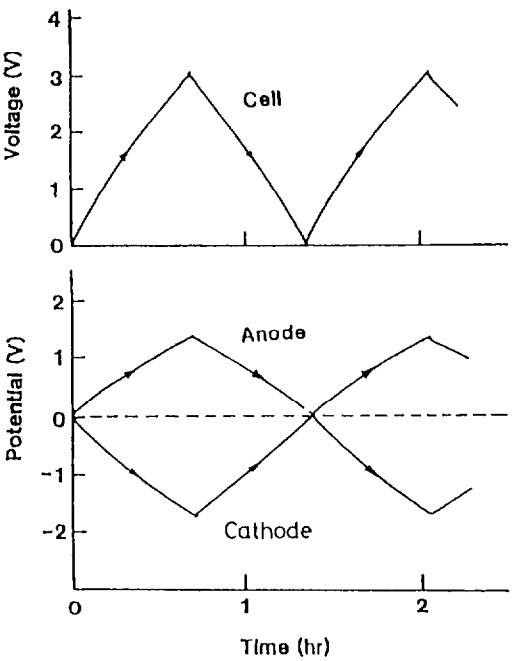

Fig. 3. Charge and discharge characteristics for the model cell in 0.5 M $(C_2H_5)_4PBF_4$/PC.

Table 1
Anode, cathode and cell capacitances in 0.5 M salt/propylene carbonate

Salt	Capacitance (F)		
	Anode	Cathode	Cell
$(C_2H_5)_4PBF_4$	3.26	2.98	1.54
$(C_3H_7)_4PBF_4$	3.26	2.83	1.49
$(C_4H_9)_4PBF_4$	3.24	2.54	1.38
$(C_6H_{13})_4PBF_4$	3.30	2.50	1.34
$(C_4H_9)_3CH_3PBF_4$	3.26	2.64	1.41
$(C_2H_5)_3(Ph\text{–}CH_2)PBF_4$	3.29	2.84	1.51
$(C_2H_5)_4PPF_6$	3.21	2.98	1.49
$(C_2H_5)_4PCF_3SO_3$	3.18	3.02	1.51
$LiBF_4$	3.55	3.07	1.63
$LiCF_3SO_3$	3.22	2.93	1.51

The specific conductivities of the solutions in the −25 to 25 °C temperature range are given in Table 2. $(C_2H_5)_4PBF_4$ and $(C_2H_5)_4NBF_4$ dissolved in PC showed the highest conductivities among the salts tested. The lithium salts in PC showed lower conductivities compared with the quarternary onium salts.

For the purpose of clarifying the electrochemical stability of the electrolyte, we observed a change in capacitance of the practical coin cell capacitor containing the electrolyte during the application of constant voltage of 2.8 V, which is required when the commercial device containing two capacitors connected in series are operated at the rated voltage of 5.5 V, as mentioned above. The capacitor containing R_4PBF_4 or R_4NBF_4 solution was found to be stable to the voltage applied at 70 °C for more than 1000 h, as shown in Fig. 4. PF_6^- or $CF_3SO_3^-$ salts of oniums showed lower stabilities compared with the corresponding BF_4^- salts. A serious degradation in capacitance was observed with the capacitor containing $LiBF_4$ or $LiCF_3SO_3$ solution.

From these, the $(C_2H_5)_4PBF_4$ solution is most suitable for use in electric double-layer capacitors because of their high conductivities, large double-layer capacitances and excellent electrochemical stability.

Table 2
Conductiviies of 0.5 M salt/propylene carbonate

Salt	Conductivity (mS/cm)		
	25 °C	0 °C	−25 °C
$(C_2H_5)_4PBF_4$	8.31	4.62	2.21
$(C_3H_7)_4PBF_4$	6.83	3.87	1.86
$(C_4H_9)_4PBF_4$	6.46	3.23	1.48
$(C_6H_{13})_4PBF_4$	4.95	2.58	1.07
$(C_4H_9)_3CH_3PBF_4$	6.52	3.76	1.65
$(C_2H_5)_3(Ph–CH_2)PBF_4$	6.44	3.40	1.72
$(C_2H_5)_4PPF_6$	7.51	4.24	1.45
$(C_2H_5)_4PCF_3SO_3$	7.15	4.12	1.97
$LiBF_4$	3.31	1.91	0.91
$LiCF_3SO_3$	1.94	0.99	0.43

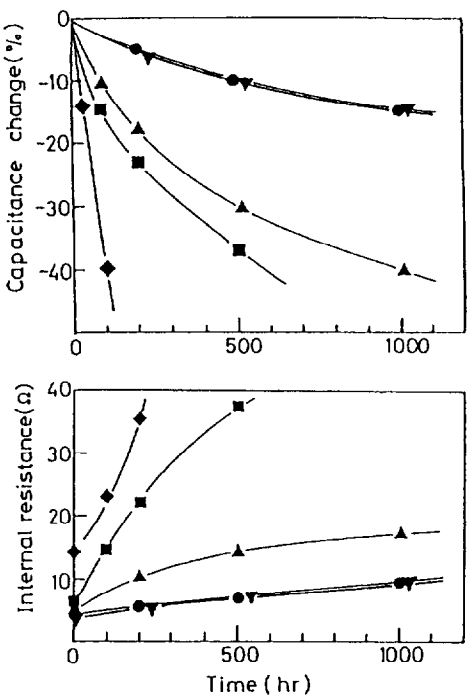

Fig. 4. Changes in capacitance of capacitors containing 0.5 M salt/PC solution during voltage application at 70 °C: (●) $(C_2H_5)_4PBF_4$; (▲) $(C_2H_5)_4PPF_6$; (■) $(C_2H_5)_4PCF_3SO_3$; (▼) $(C_2H_5)_4NBF_4$; (◆) $LiBF_4$.

2.2.2. Electrode

It is required that an activated carbon electrode neither react with the electrolyte nor be oxidized and reduced by itself at the anodic and cathodic polarization potential. Since the voltage is constantly applied to the EDLC for memory protection use, remarkable deterioration in performance occurs after long-term voltage application even if the current caused by the electrochemical decomposition reaction is extremely small. It is expected that the electrochemical stability of an activated carbon electrode against voltage application is influenced by the surface property of activated carbon.

Activated carbon samples with various pore structures were prepared by controlling the condition of activating processes. The specific surface area and pore volume of activated carbons prepared from coconut shell, phenol resin and petroleum coke were measured by the BET method and Clanston–Inkley method, respectively. Disc electrodes were prepared by mixing an activated carbon pulverized below #200 mesh with a carbon black and PTFE, kneading, extruding, rolling to a 0.55 mm thick sheet and punching out. The apparent density and porosity of the disc electrode were evaluated from the weight and the true volume of the electrode obtained by immersing the electrode in PC under a pressure of 1 Torr and measuring the PC volume increase. The performance of the capacitors and their relationships with the electrodes properties comprising various activated carbons were studied by fabricating practical coin cell capacitors.

Table 3 lists the BET surface area and the pore volume of the activated carbon samples studied. Table 4 gives the properties of the PTFE-bonded activated carbon electrodes and the performance of the capacitor using the electrodes and

Table 3
BET surface area, total pore volume of activated carbon samples

Raw material	Sample no.	Surface area (m^2/g)	Pore volume (cm^3/g)
Coconut shell	Y1	960	0.46
	Y2	1290	0.58
	Y3	1620	0.79
	Y4	1860	0.97
	Y5	2060	1.12
Phenol resin	P1	2100	1.00
	P2	2350	1.31
Petroleum coke	K1	2600	1.39
	K2	2770	1.50
	K3	2890	1.65
	K4	3100	1.78

Table 4
Properties of PTFE-bonded activated carbon electrodes and performance of capacitor using these electrodes

Activated carbon sample no.	Properties of PTFE-bonded electrode			Performance of capacitor	
	Apparent density (g/cm^3)	Porosity (%)	Weight of disc electrode (mg)	Capacitance (F)	Internal resistance (Ω)
Y1	0.68	67.3	12.4	0.326	17.1
Y2	0.66	66.7	12.1	0.491	14.5
Y3	0.62	68.1	11.3	0.532	15.7
Y4	0.49	74.1	9.0	0.484	15.3
Y5	0.47	75.1	8.7	0.479	16.4
P1	0.55	71.5	9.9	0.544	17.8
P2	0.46	75.0	8.3	0.509	18.2
K1	0.49	76.7	9.0	0.560	20.1
K2	0.44	77.2	8.0	0.500	19.0
K3	0.45	78.5	7.4	0.522	15.3
K4	0.38	80.8	6.3	0.506	17.1

$(C_2H_5)_4PBF_4$/PC as the electrolyte. All electrodes were composed of 80 wt.% activated carbon, 10 wt.% carbon black and 10 wt.% PTFE. From the data, correlations between capacitances of the electrode and the pore properties of activated carbons were studied [4]. Fig. 5 shows the relationship between the volumetric capacitance of PTFE-bonded activated carbon electrode and the surface area of the activated carbon. Fig. 6 shows the relationship between the gravimetric capacitance of the electrode and the surface area of the activated carbon. The volumetric capacitance which determines the energy density of the capacitor shows its maximum at a surface area of 2000–2500 m^2/g, and decreases as the surface area increases over 2500 m^2/g. As shown in Fig. 7, as the specific surface area increases, the pore volume of activated carbon increases and the apparent density of the electrode decreases. As the volumetric capacitance is a function of the apparent density and the surface area, the maximum volumetric capacitance is attained by the compromise between the increase in the surface area and the decrease in the apparent density. On the other hand, the gravimetric capacitance increases linearly with the increase in the surface area. These facts suggest that the double-layer capacitance of the unit area of activated carbons is constant and independent of the kind of carbon species and the pore structure of activated carbon.

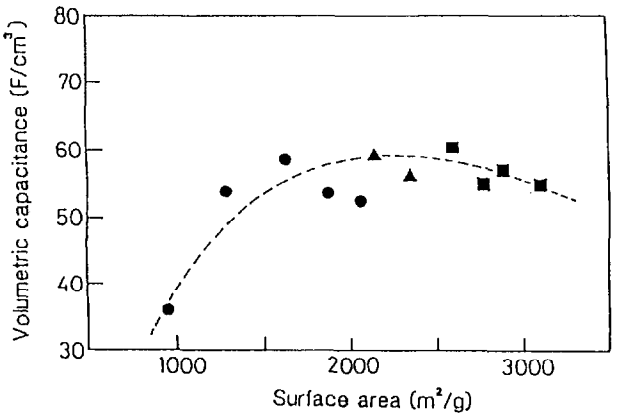

Fig. 5. Volumetric capacitance of PTFE-bonded carbon electrode vs. surface area of activated carbon used for the electrode.

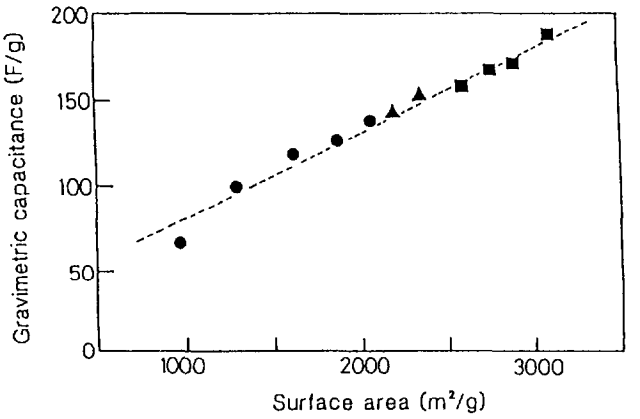

Fig. 6. Gravimetric capacitance of activated carbon contained in the electrode vs. surface area of activated carbon.

Stabilities against applied voltage and the relationship with the kind of activated carbon electrode were evaluated under a condition of accelerating deterioration, using coin cell capacitor. Fig. 8 shows the change in capacitance and internal

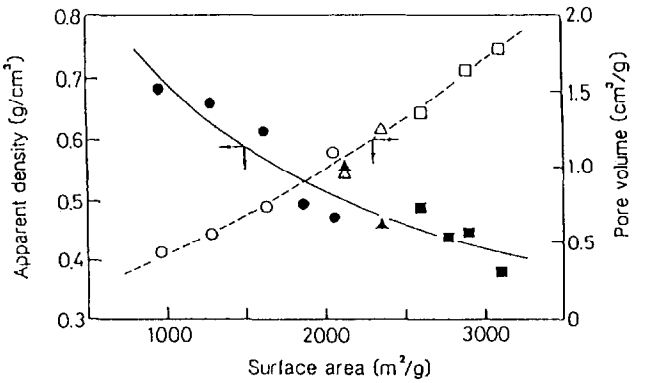

Fig. 7. Correlation between surface area of activated carbon and apparent density of the electrode, and pore volume of activated carbon.

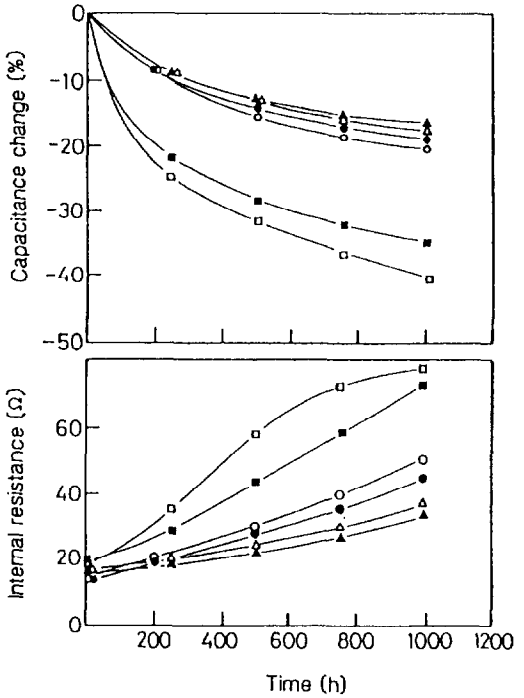

Fig. 8. Changes in capacitance and internal resistance of capacitor during voltage application of 2.8 V at 70 °C: (●) Y3; (○) Y5; (▲) P1; (■) P2; (■) K1, and (□) K4.

resistance of the capacitor during the application of 2.8 V at 70 °C. The cells comprising electrodes fabricated with the activated carbons prepared from coconut shell and phenol resin showed comparatively stable performances, whereas the cells containing the activated carbons prepared from petroleum cokes showed a great deterioration in capacitance and a great increase in internal resistance after 1000 h of voltage application. It was found that the deteriorated cells showed large expansion arising from gas evolution caused by the electrochemical decomposition of PC.

It is expected that the electrochemical decomposition of PC is strongly related with the existence of oxygen-containing functional groups, such as carboxylic and quinone groups, on the surface of activated carbons. So the influence of the oxygen content of the activated carbon used for the electrode on the capacitance change of the capacitor after voltage application of 2.8V at 70 °C for 1000 h was studied.

As shown in Fig. 9, the deterioration of the coin cell after the voltage application becomes small as the oxygen content of activated carbon becomes small. These facts suggest that the removal of the functional groups from the surface of activated carbon is an effective way to obtain stable performance of the capacitor during voltage application.

2.2.3. Cell container

During charging, a voltage of 2.8 V is applied to the unit cell of EDLC-containing organic electrolyte. The anode-side materials, such as current collector and cell container material, are at high positive potential and must show resistance towards electrochemical corrosion [5]. Although precious

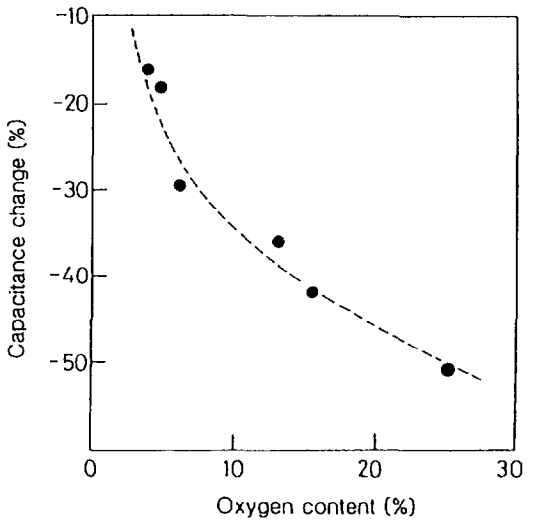

Fig. 9. Influence of oxygen content of activated carbon used for electrode on capacitance change after voltage application of 2.8 V at 70 °C for 1000 h.

metals, valve metals such as Al, Ti, Ta, and carbon material are resistant against anodic polarization, most of these do not have enough mechanical strength or low cost required to form practical coin cells. As the electrode potential of the anode-side activated carbon electrode in EDLC is expected 3 V higher than that of the positive electrode, stainless-steel SUS 304, which is widely used in lithium batteries, corroded severely during anodic polarization and was inadequate as the anode-side material. To find new alloys suitable as cell container or current collector, the dissolution potential and the weight loss of new stainless steels, iron–nickel alloys and nickel alloys are studied, by anodically polarizing the alloys in PC solution.

Alloys for use as container (current collector) were abraded by emery paper and irradiated by ultrasonic wave in acetone. In a glove box filled with nitrogen kept at a dew point below −50 °C, the alloy electrodes with an area of 1 cm^2 were anodically polarized under a constant current in a PC solution of $(C_2H_5)_4PBF_4$ using nickel (25 cm^2) as the counter electrode and a silver mesh as the reference electrode. The dissolution potential was determined by extrapolating the potential–current curve to zero current.

The activated carbon electrode (diameter: 20 mm, thickness: 0.5 mm) was stuck to one surface of the cathode metal current collector (diameter: 20 mm, thickness: 0.2 mm) using conductive carbon adhesives, and dried for 3 h at 300 °C in vacuum. Then, platinum–lead wires were attached to the backside of the current collector, which was covered with a PTFE sheet. A constant voltage of 2.8 V was applied between the anode current collector and the nickel cathode current collector with the same activated carbon electrode in 0.5 M PC solution of $(C_2H_5)_4PBF_4$. After a few hundred hours of voltage application, the weight loss of the anode current collector was measured.

Table 5 shows the composition of various alloys used for the measurement of dissolution potential. These alloys stud-

Table 5
Composition of alloy samples used for cell container

Alloy	Contents (wt%)							
	Fe	Cr	Ni	Mo	Cu	Ti	Co	W
SUS304	71.2	18.0	8.4					
SUS316L	67.0	16.3	12.3	2.0				
S-1	54.7	22.1	17.2	4.6				
FN-1	41.5	20.1	29.0	2.3	3.9			
FN-2	31.6	21.6	39.6	3.0	2.3	1.0		
N-1	8.4	15.4	75.3		0.1			
N-2	5.2	15.4	58.9	15.5			0.7	0.7
N-3	1.1		63.8		33.8			

ied were the commonly used stainless-steel SUS316L, more corrosion resistant austenite-type special stainless steel, S-1, high corrosion resistant Fe–Ni alloy, FN-1 and FN-2, which were originally developed for chemical plants, and the especially high corrosion resistant Ni alloys, N-1, N-2 and N-3. Anodic current–potential curves of these alloys in $(C_2H_5)_4PBF_4$/PC solution are shown in Fig. 10.

As shown in Fig. 10, the dissolution potential versus silver was determined by extrapolating the potential–current curve to zero current. Dissolution potential of the alloys studied are summarized in Table 6. SUS304 showed the most negative dissolution potential. The dissolution potential of S-1 was 1.7 and 1.1 V higher than those of SUS304 and N-1, respectively. In Table 6, the dissolution rates estimated from weight loss after the application of 2.8 V to the cell for a fixed period are also summarized. Neither weight loss nor surface change were observed in the alloys S-1 and FN-1. On the other hand, weight loss caused by the electrochemical dissolution and formation of small pores by electrochemical pitting was observed in alloys which have a more negative dissolution potential than that of FN-1. Further S-1 and FN-1 showed enough mechanical strength and tenacity to obtain coin cells of good sealing and to keep the electrolyte solution in the cell.

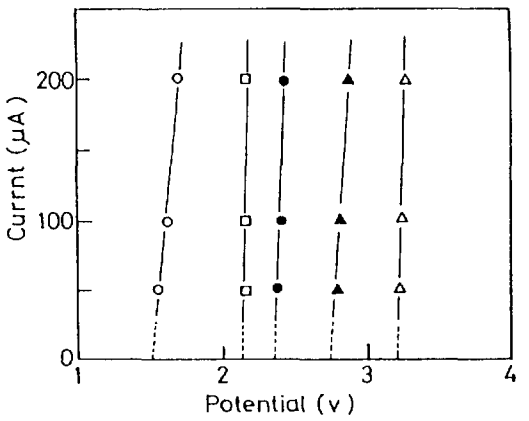

Fig. 10. Anodic current–potential curves in $(C_2H_5)_4PBF_4$/PC: (○) SUS304; (●) SUS316L; (■) S-1; (▲) FN-1, and (□) N-1.

Table 6
Anodic dissolution potential and anodic dissolution rate of alloys in $(C_2H_5)_4PBF_4$/propylene carbonate

Sample no.	Dissolution potential [a] (V vs. Ag)	Dissolution rate [b] (mg/(100 h cm^2))
SUS304	1.54	238.9
SUS316L	2.42	3.8
S-1	3.23	0.0
FN-1	2.80	0.0
FN-2	2.41	10.1
N-1	2.16	4.7
N-2	2.32	7.5
N-3	2.22	12.9

[a] V vs. Ag, determined from polarization curves by extrapolating the linear potential vs. current plot to zero current.
[b] Estimated from the weight loss at constant applied voltage of 2.8 V.

2.3. Performance

The performance of the stacked coin cell comprising the materials mentioned before was tested.

The performance of the electric double-layer capacitor is defined in terms of capacitance, CAP, leakage current, LC, and equivalent series resistance, ESR.

The capacitor was charged at a rated voltage of 5.5 V, then discharged at a constant current. A capacitance value is calculated from $C = IT/\Delta V$, where C is the capacitance value in F, I the discharge current in A, T the time for discharge in s and ΔV the voltage change of the cell caused by discharge in V.

The internal resistance is termed equivalent series resistance (ESR) in the electric double-layer capacitor. Among the components contributing to the ESR are the resistance of the electrolyte in the microporous separator and that of the electrodes.

When the voltage is applied to the capacitor, three different kinds of current flow through the capacitor and decrease with time. First, the charging current flows to store charge electrostatically. After a time, the absorption current flows to supply charge that is not recovered upon discharge of the capacitor. Finally, only the leakage current flows through the cell. Due to ultra-high capacitance of the electric double-layer capacitor, it takes about 30 h to reach a steady current: i.e. the leakage current. The magnitude of this current will determine the rate of self-discharge. We specify the leakage current as the current measured 30 min after the voltage application started. A leakage current, aside from mechanical faults such as a separator rupture, is the result of impurities in the electrolyte and the electrode, surface species of the electrode participating in charge-transfer processes and the corrosion of the alloy container. The leakage current of our electric double-layer capacitor is reduced by utilizing materials of high purity and stability.

Fig. 11 shows the relationship between the retained voltage and self-discharge time as a function of the capacitance of the products. More than 4.0 V is retained during 100 h self-discharge time.

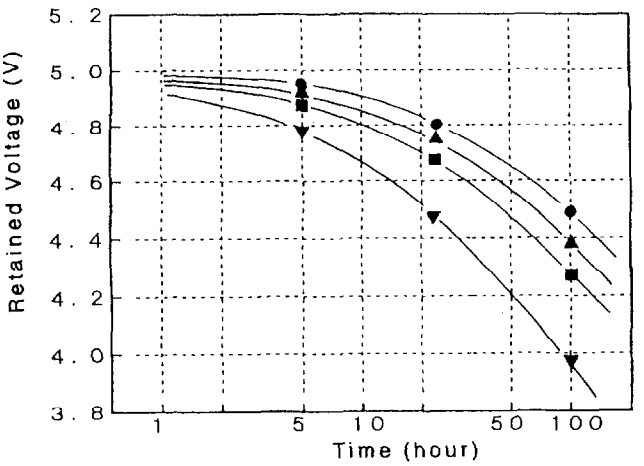

Fig. 11. Voltage retention for two-cell stacked capacitors after charging by constant volatage application of 5.0 V: (●) 1 F; (▲) 0.47 F; (■) 0.1 F, and (▼) 0.047 F.

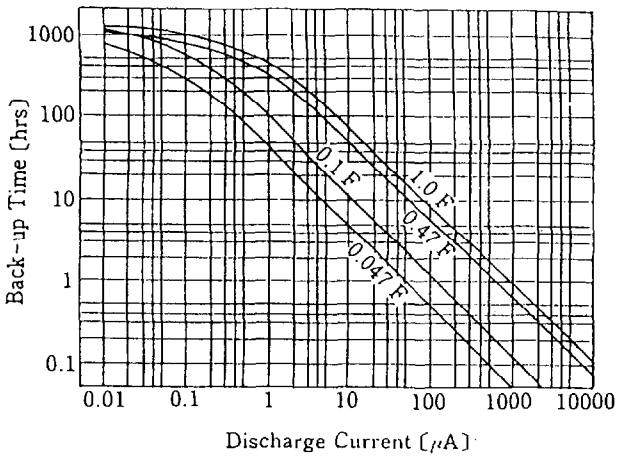

Fig. 12. Backup time vs. discharging current.

The CMOS RAM memory can be maintained in most cases if the voltage is above a threshold value of 2.0 V. The time for the capacitor voltage to fall from its initial value of 5.0 V to the threshold value is called 'backup time'. Fig. 12 shows the minimum backup time capabilities for constant discharge current. The real backup time, when discharged with a CMOS microcomputer, is longer than the time shown in Fig. 12. The reason for this is that when the capacitor is used as a power backup source for microcomputers, the backup current falls sharply due to the fall of the voltage.

Tests to evaluate the change in capacitance and ESR of EDLC after 1000 h of operation at a temperature of 70 °C applying a voltage of 5.5 V indicated a capacitance decrease of less than 20%, as shown in Fig. 13.

Fig. 14 shows charge and discharge cycle-life test at a temperature of 70 °C. The capacitance decrease is less than 15% after 10 000 times repetition of charging for 10 min at constant voltage of 5.5 V and discharging for 10 min with 100 Ω series resistance.

The results show that the electric double-layer capacitor exhibits excellent stability against repetition of charge discharge cycle.

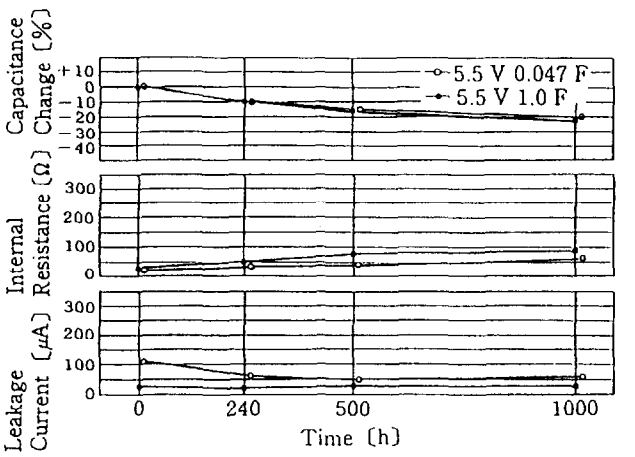

Fig. 13. Reliability of performance during voltage application of 5.5 V at 70 °C.

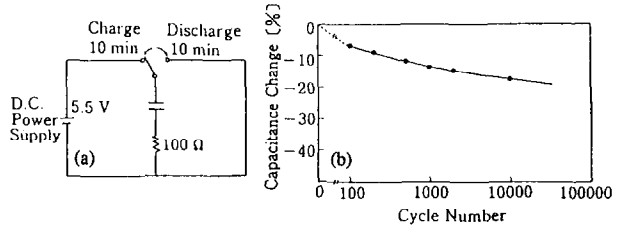

Fig. 14. Cycle-life performance at 70 °C: (a) circuit diagram for charge/discharge cycling, and (b) capacitance change during cycling.

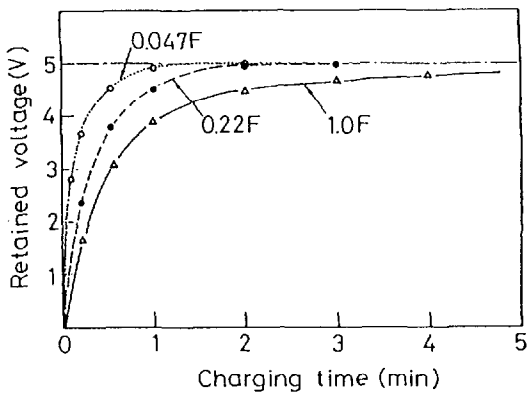

Fig. 15. Retained voltage vs. charging time.

As shown in Fig. 15, the electric double-layer capacitor is charged fully in 5 min at constant voltage charging. From these results, it is seen that quick charging and discharging is possible.

2.4. Application of the coin-type capacitor

The coin-type capacitor is used to provide memory backup for devices during an interruption of commercial alternative current in many electric applications such as video tape recorders, measuring equipment, etc. The capacitors combined with solar cells are useful as electric sources for watches and radios.

The capacitors also work as electric power sources during the replacement of the primary battery in pagers and cameras.

3. Power capacitor

3.1. Construction

Using almost the same materials as those of coin-type capacitor, a power capacitor, as shown in Fig. 16, has been developed. The power capacitor consists of activated carbon sheet electrodes attached to aluminum foil current collectors and non-woven fabric separator. Rectangular polarizable anodes and cathodes separated by non-woven fabric separators are stacked alternatively. These electrodes are electrically connected to terminals by current lead.

The whole assembly immersed in an organic electrolyte solution is housed in a stainless-steel box of 112 mm × 127 mm × 30 mm.

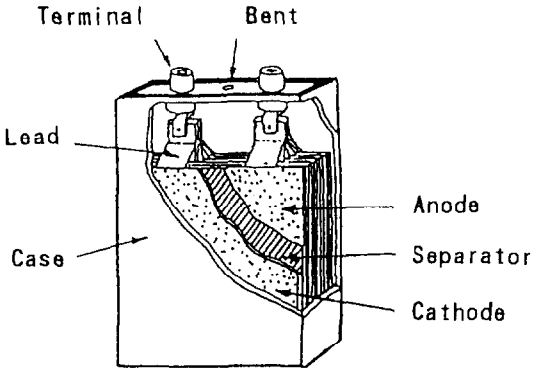

Fig. 16. Setup of power capacitor.

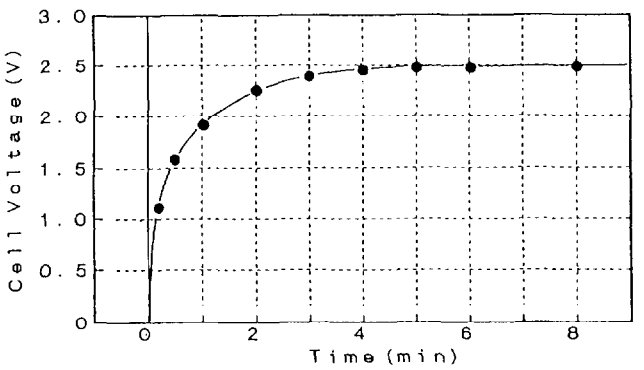

Fig. 17. Charging characteristic of 4300 F power capacitor.

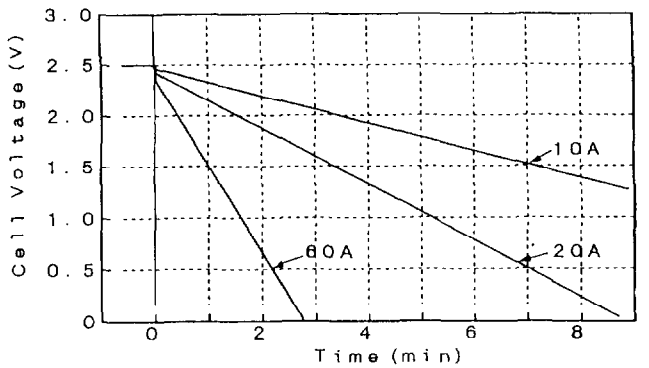

Fig. 18. Discharging characteristic of 4300 F power capacitor.

3.2. Performance of the power capacitor

Fig. 17 shows the charge characteristics of the 4300 F capacitor. The capacitor can be fully charged within 5 min under constant voltage charging of 2.5 V.

Fig. 18 shows the discharge characteristics of the capacitor. The cell voltage of the capacitor decreases linearly under

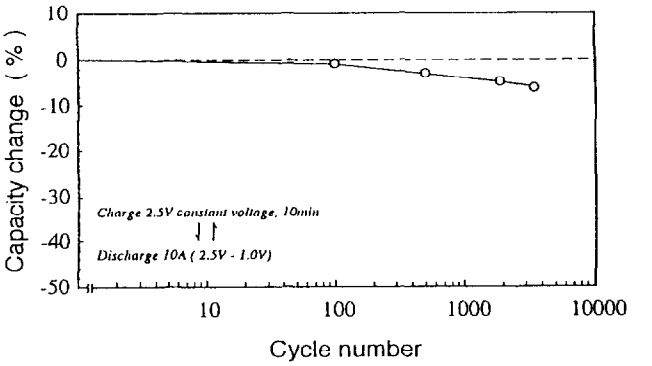

Fig. 19. Cycle-life performance of 4300 F power capacitor.

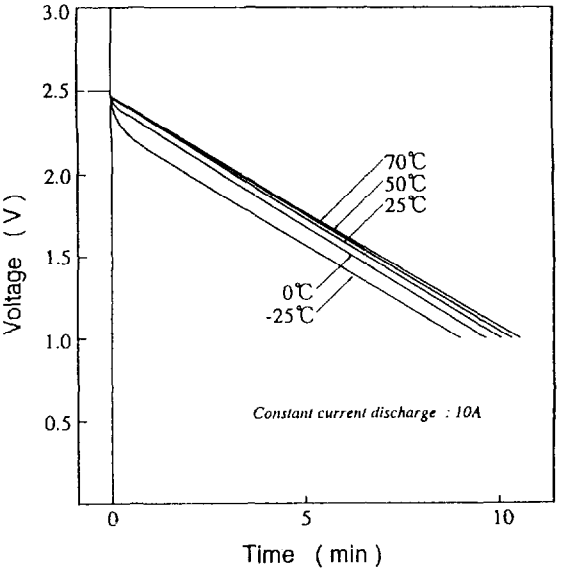

Fig. 20. Temperature performance of 4300 F power capacitor.

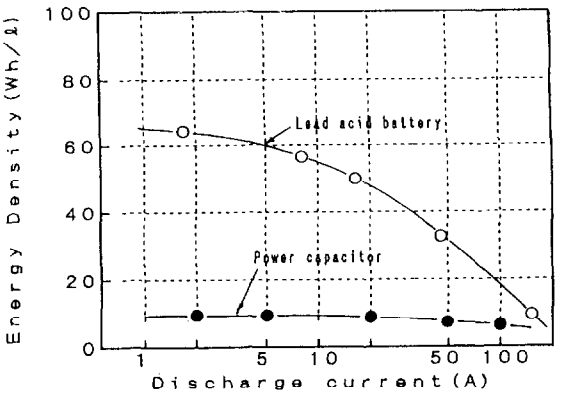

Fig. 21. Comparison of energy density between 4300 F power capacitor and lead/acid battery (16 Ah, 12 V) as a function of discharge current: (●) power capacitor, and (○) lead/acid battery.

constant discharge current from 2.5 to 1.0 V in 300 s or in 90 s for discharge currents of 20 or 60 A, respectively.

Fig. 19 shows the cycle-life performance of the cell. The capacitance of the cell is maintained constant over 3000 times repetition of charging for 10 min under constant voltage of 2.5 V and discharging under constant current of 10 A from 2.5 to 1.0 V. Fig. 20 shows the temperature performance of the capacitor. Voltage decrease slopes under constant discharge current show that the capacitance change is small in the temperature range from −25 to 70 °C.

Fig. 21 compares the energy density of the capacitor with that of a small lead/acid battery commercially produced.

As the discharge current of the lead/acid battery is limited by ion diffusion, the energy density of the lead/acid battery becomes smaller at high discharge current compared with that of the capacitor, which provides practical applications where a large current is needed for a short period.

4. Summary

The materials and the performance of two kinds of electric double-layer capacitor with organic electrolyte were outlined.

The first one is a coin-type and the second a rectangular-type capacitor.

The coin-type capacitor is composed of a couple of electrodes fabricated with an activated carbon having high surface area and low oxygen content, a solution of $(C_2H_5)_4PBF_4$ dissolved in PC and a high corrosion resistant alloy container. The capacitor is fabricated from two unit cells stacked in series, and is capable of being operated at a voltage up to 5.5 V. Since the operation of the capacitor is based on an electrostatic phenomenon, the operational life should not be affected by electrochemical processes, which limit the cycle live of secondary batteries. In practice, deep charge/discharge cycling more than 10 000 times and storage for a long period do not affect the performance. The design of the capacitor is suitable for power sources for memory protection.

The rectangular-type cell composed of almost the same materials as those of the coin-type capacitor shows the extremely high capacitance of 4300 F and low d.c. resistance. The performance of the rectangular-type capacitor offers access to applications which are used at a high charge/discharge rate .

References

[1] T. Morimoto, K. Hiratsuka, Y. Sanada, K. Kurihara, S. Ohkubo and Y. Kimura, *Proc. 33rd Int. Power Sources Symposium, Cherry Hills, USA, 1988*, p. 618.

[2] K. Hiratsuka, T. Morimoto, Y. Sanada and K. Kurihara, *Ext. Abstr., 178th Meet. The Electrochemical Society, Seattle, WA, USA, 1990*, Vol. 90-2, p. 129.

[3] K. Hiratsuka, Y. Sanada, T. Morimoto and K. Kurihara, *Denki Kagaku, 59* (1991) 209.

[4] K. Hiratsuka, Y. Sanada, T. Morimoto and K. Kurihara, *Denki Kagaku, 59* (1991) 607.

[5] K. Hiratsuka, H. Aruga, Y. Sanada, T. Morimoto and K. Kurihara, *Denki Kagaku, 59* (1991) 897.